Available online at www.sciencedirect.com
ScienceDirect
Trans. Nonferrous Met. Soc. China 26(2016) 2653−2664
Transactions of Nonferrous Metals Society of China
www.tnmsc.cn

Effect of ZrC−SiC content on microstructure and ablation properties of C/C composites

Jun LI, Xin YANG, Zhe-an SU, Liang XUE, Ping ZHONG, Shuai-peng LI, Qi-zhong HUANG, Hong-wei LIU

State Key Laboratory of Powder Metallurgy, Central South University, Changsha 410083, China

Received 10 October 2015; accepted 18 May 2016

Abstract: C/C−ZrC−SiC composites with different ZrC−SiC contents were fabricated by precursor infiltration and pyrolysis. The effect of ceramic content on the microstructure and ablation resistance was investigated. Both the C/C−SiC and C/C−ZrC−SiC composites exhibited good ablation resistance under the plasma flame above 2300 °C. With the increase of ZrC content, a continuous oxide layer and a solid Zr−Si−O mesophase were formed during the ablation. And the structure of the formed oxides layer closely linked with the contents of ZrC−SiC ceramics. The solid ZrO_2−ZrC and Zr−Si−O mesophase could increase the viscosity of SiO_2 moderately and improve the anti-scouring ability. The continuous SiO_2−ZrO_2−ZrC−SiC layer would serve as a thermal and oxygen barrier for preventing the substrate from further ablation. The C/C−ZrC−SiC composites with 27.2% ZrC and 7.56% SiC shows superior ablation resistance, and the mass and linear ablation rates are −3.51 mg/s and −1.88 μm/s, respectively.
Key words: C/C composites; ZrC; SiC; ablation; precursor infiltration and pyrolysis

1 Introduction

Carbon/carbon (C/C) composites have many excellent properties like light weight, exceptional high temperature strength and good resistance of thermal shock and ablation. These characteristics enable them to be an ideal material for using in aerospace such as solid rocket motor, leading edges of reentry vehicles and rocket nosetip [1−3]. However, with the development of hypersonic aircraft, the materials are desired to resist oxidation and be re-usable in oxygenous environment over 2000 °C. But the properties of current C/C or C/C−SiC composites are far from satisfactory, owing to their sensitivity to oxidation at high temperature [4,5]. To improve the ablation resistance of C/C composites, ultra-high temperature ceramics (UHTCs) such as refractory carbides/borides modified C/C composites have been developed in recent years [6−10]. Among these UHTCs, ZrC−SiC composites have attracted much attention because of the high melting point of ZrC (3540 °C) and its oxide ZrO_2 (2770 °C), good chemical inertness, relatively low density and good ablation resistance [11,12]. Moreover, the formed molten binary oxides ZrO_2−SiO_2 could seal cracks to protect the internal matrix and fibers [13].

In the past few years, intense efforts have been focused on introducing ZrC−SiC ceramics into C/C composites. XIE et al [14,15] demonstrated that ZrC−SiC doped C/C composites prepared by precursor infiltration and pyrolysis (PIP) process had excellent ablation resistance, and investigated the influence of cyclic ablation on the ablation behavior and morphology of the composites. LI et al [16] reported a new technique to fabricate C_f−ZrC−SiC composites through vapor silicon infiltration (VSI) process. YANG et al [17] added ZrC−SiC into C/C composites by reactive melt infiltration (RMI) with Zr, Si mixed powders as raw materials. Meanwhile, ZHANG et al [18] and LIU et al [19] fabricated the C_f−ZrC−SiC composites with combination of PIP and RMI. However, the effect of ZrC−SiC content on ablative performance of C/C composites was rarely reported. Actually, the contents of ZrC and SiC ceramics will influence the structure and ablation resistance of the composites significantly. FENG et al [20] indicated that the ablation rates of C/C−ZrC−SiC composites decreased rapidly until the mass ratio of SiC/ZrC reduced to 1:1.5, and then turned

Foundation item: Project (2011CB605801) supported by the National Basic Research Program of China; Project (51304249) supported by the National Natural Science Foundation of China; Project (2013BAE04B02) supported by the National Key Technology Support Program of China; Project (14JJ3023) supported by the Hunan Provincial Science Foundation of China
Corresponding author: qi-zhong HUANG; Tel: +86-731-88877671; Fax: +86-731-88836078; E-mail: qzhuang@ csu.edu.cn
DOI: 10.1016/S1003-6326(16)64392-3

to rise with the SiC/ZrC ratio continuously decreasing. While YAN et al [21] reported that it would degrade the ablation property with the increase of SiC content. Therefore, it is necessary and significant to study the ablation characteristic of C/C−ZrC−SiC composites with different ZrC−SiC contents. Besides, many researchers focused on the ablation properties of C/C−ZrC−SiC composites under oxyacetylene torch at 3000 °C. At this temperature, the formed ZrO_2−SiO_2 film has good self-healing ability due to the melting of ZrO_2−SiO_2 particles. However, the ablation behavior and mechanism of C/C−ZrC−SiC composites at lower temperature were not fully understood. In the temperature range of 2300−2700 °C, which is above the boiling point of SiO_2 (2230 °C) while below the melting point of ZrO_2 [22] and the sublimation temperature of SiC(2700 °C) [23], the ablation behavior and mechanism of C/C−ZrC−SiC composites may be quite different. So, it is necessary to study the ablation mechanism of C/C−ZrC−SiC composites with different ZrC−SiC contents at 2300 °C.

In the present study, C/C−ZrC−SiC composites with different ZrC and SiC contents were fabricated by PIP using SiC precursor and zirconium-containing precursor separately. The controllable ceramic content had been achieved. And the influence of different ZrC and SiC contents on microstructure and ablation resistance of C/C composites was investigated. Meanwhile, effect of ZrC−SiC content on the structural evolution of the formed oxides layer was discussed, and the ablation mechanism under the plasma flame was proposed.

2 Experimental

2.1 Material preparation

2.5D needled felts with a density of 0.45 g/cm^3 were deposited with prolytic carbon by chemical vapor infiltration (CVI) process. Afterwards, the porous C/C composites with a density of 1.45 g/cm^3 were modified with ZrC−SiC ceramics by PIP process. Zirconium acetate ($C_8H_{12}O_8Zr$) (Aladdin Industrial Corporation, Shanghai, China) was used as ZrC precursor. SiC was obtained via pyrolysis of SiC precursor (Central South University, Changsha, China). The porous C/C composites were firstly infiltrated with SiC and ZrC precursors, and then pyrolysed at 1500−1700 °C for 1 h in a flowing argon atmosphere. Zirconium acetate in the felts was firstly decomposed to ZrO_2 during the high temperature treatment, then converted into ZrC through carbothermal reduction reaction between ZrO_2 and carbon as Eq. (1). In order to accurately calculate the content of SiC and ZrC respectively, only one precursor was used during each PIP cycle and the mass gain in each cycle was recorded. Then, the content of the introduced ZrC/SiC ceramics is calculated by the accumulated mass gain for each precursor. The PIP process was repeated for a number of times until the density was above 2.0 g/cm^3. And C/C−ZrC−SiC composites with different ceramic contents were obtained, which were C/C−7.56%SiC−27.2%ZrC and C/C−18.77%SiC−10.21%ZrC, marked as CSZ-H and CSZ-L, respectively. C/C−SiC composites were prepared with SiC precursor for the same PIP cycles.

$$ZrO_2(s)+3C(s)=\!=ZrC(s)+2CO(g) \quad (1)$$

2.2 Ablation test

The ablation tests were conducted using a plasma generator equipment (Muitiplaz 3500) with cylindrical-shaped samples (d30 mm × 10 mm) which were cut from the prepared composites. The working voltage and current of the plasma generator were (160±1) V and 6 A, respectively [24]. The distance from the plasma gun tip to the surface of the specimen was about 10 mm, and the inner diameter of the gun tip was 2 mm. Surface temperature of the ablation center of the samples reached as high as 2300 °C, as monitored by an optical pyrometer. During the test, the orientation of the flame was vertical to the surface of the sample and the ablation time was 60 s. The mass and linear ablation rates were obtained as an average of three samples by the following formula:

$$R_{\mathrm{m}}=\frac{m_0-m_t}{t} \quad (2)$$

$$R_{\mathrm{l}}=\frac{l_0-l_t}{t} \quad (3)$$

where, R_{m} and R_{l} donate the mass ablation rate (mg/s) and linear ablation rate (μm/t), respectively; m_0 and l_0 donate the mass and thickness of the sample before ablation, respectively; m_t and l_t donate the mass and thickness at the ablation center of the sample after ablation, respectively; t donates the test time. The thickness and mass of the sample were measured by spiral micrometer and analytical balance, respectively.

2.3 Characterization

The densities of the composites were obtained by Archimedes method. The morphologies of the prepared composites were investigated by scanning electron microscopy (SEM, FEICO, NOVA, Nano230) equipped with energy dispersive spectroscopy (EDS). Phase analysis was conducted using an X-ray diffraction (XRD) analyzer (Rigaku Ltd. Japan. Cu K_α radiation). Electron probe microanalysis (EPMA, JEOLCO, JXA8530F) was used to detect distributions of the primary elements in the composites.

3 Results and discussion

3.1 Microstructure of prepared composites

The typical XRD patterns of the prepared composites are shown in Fig. 1. It can be found that SiC is the only crystal phase in C/C−SiC composites, while ZrC and SiC are the main crystal phases in CSZ-H and CSZ-L. For the C/C−SiC composites, the strong intensity peaks at 35.6°, 41.4°, 59.9°, 71.7° and 75.5° were matched to (111), (200), (220), (311) and (222) planes of SiC according to the JCPDS card No. 29−1129. For C/C−ZrC−SiC composites, the peaks at 33.02°, 38.32°, 55.28°, 65.92° and 69.28° match well with planes of ZrC (JCPDS card No. 65−0332), and the XRD patterns indicated that ZrO_2 had been completely converted into ZrC after the high temperature treatment. In addition, the narrow and sharp peaks inferred good crystallization of SiC and ZrC phase. It is worthwhile to notice that the intensity of ZrC diffraction peak is stronger than that of SiC in CSZ-H, while it is just the opposite in CSZ-L. What's more, there are more carbon in C/C−SiC composites compared with CSZ-H and CSZ-L, because part of the carbon reacted with ZrO_2 in C/C−ZrC−SiC composites at high temperature.

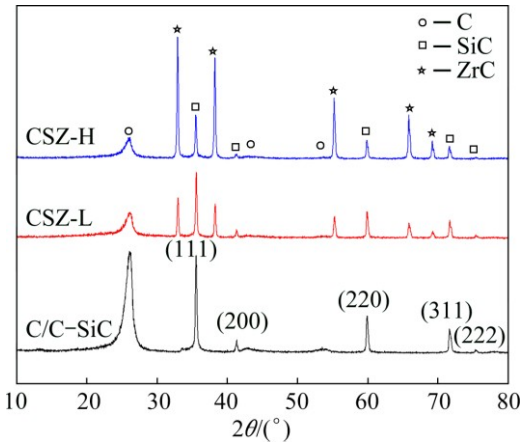

Fig. 1 XRD patterns of C/C−SiC and C/C−ZrC−SiC composites with different ZrC−SiC contents

Figure 2 shows the cross-section microstructure of C/C−SiC and C/C−ZrC−SiC composites. As shown in Figs. 2(a), (c) and (e), the composites are almost compact with ZrC and SiC ceramics filling the pores after high temperature heat treatment. The formed massive ceramics are mainly concentrated in the short-cut fiber layers (Fig. 2(a)) due to a large number of big pores exist in these layers. Figures 2(b), (d) and (f) display the microstructure of intra-bundle areas and the morphology of ceramic particles in corresponding composites with the insert figures in upper right corner. It is obvious that ZrC−SiC ceramics were evenly distributed in the intra-bundle areas, which indicates that the precursors of SiC and ZrC have excellent fluidity. However, some micro-pores and micro-cracks still remained in the intra-bundle areas because of the different coefficients of thermal expansion [25] and the blocking effect resulting from the pyrolysis of precursors [26]. Among Figs. 2(b), (d) and (f), the micro-pores and micro-cracks in CSZ-H and CSZ-L are less than those in C/C−SiC composites, and the amount of close pores is higher in CSZ-L compared with CSZ-H. The reason of this phenomenon can be attributed to the lower viscosity of zirconium acetate than SiC precursor, so the ZrC precursor could infiltrate into intra-bundle areas more easily. Additionally, the sizes of the ceramic particles in CSZ-H and CSZ-L are also smaller than that in C/C−SiC composites, and ceramic particle aggregation is found in CSZ-L and C/C-SiC composites. So it could be concluded that the ZrC particles are helpful for inhibiting the growth of SiC grains.

To further study the microstructure and elemental distribution of the prepared composites, EPMA was used to investigate the cross-section of the prepared composites. Figures 3 and 4 show the morphology and element analysis results of C, Si and Zr in CSZ-H and CSZ-L, respectively. As can be seen in Figs. 3(a) and 4(a), some ZrC−SiC hybrid ceramics were embedded circle-around carbon fiber, which demonstrated that the precursor of SiC and ZrC could infiltrate into the micro-cracks caused by thermal mismatch between carbon fiber and pyrocarbon [27]. Meanwhile, the pores of matrix were sealed by the hybrid ceramics. The content of Zr is obviously higher than that of Si in CSZ-H from Figs. 3(c) and (d), while the content of Si is higher than that of Zr in CSZ-L as shown in Figs. 4(c) and (d). Combined with the results of XRD patterns in Fig. 1, it further confirms that the contents of ZrC and SiC are obviously different in CSZ-H and CSZ-L.

The cross-section morphology and elemental distribution of C/C−SiC are shown in Fig. 5. Despite some micro-pores were found in the matrix (Fig. 5(a)), the SiC ceramics were distributed relatively homogeneously among matrix and interspace of carbon fiber and pyrocarbon just like Figs. 3(a) and 4(a). The integration of SiC ceramics and pyrocarbon can inhibit the inward diffusion of oxygen when ablation occurs.

According to the results of XRD, SEM and EPMA images, the C/C−SiC and C/C−ZrC−SiC composites with different SiC and ZrC contents had been fabricated by separating the precursor during the PIP process. Thus, the controllable content had been achieved. The SiC and ZrC ceramics were embedded around carbon fibers and filled the large pores in matrix. On one hand, the compact matrix ceramics can effectively improve the density of the C/C composites. On the other hand, it is

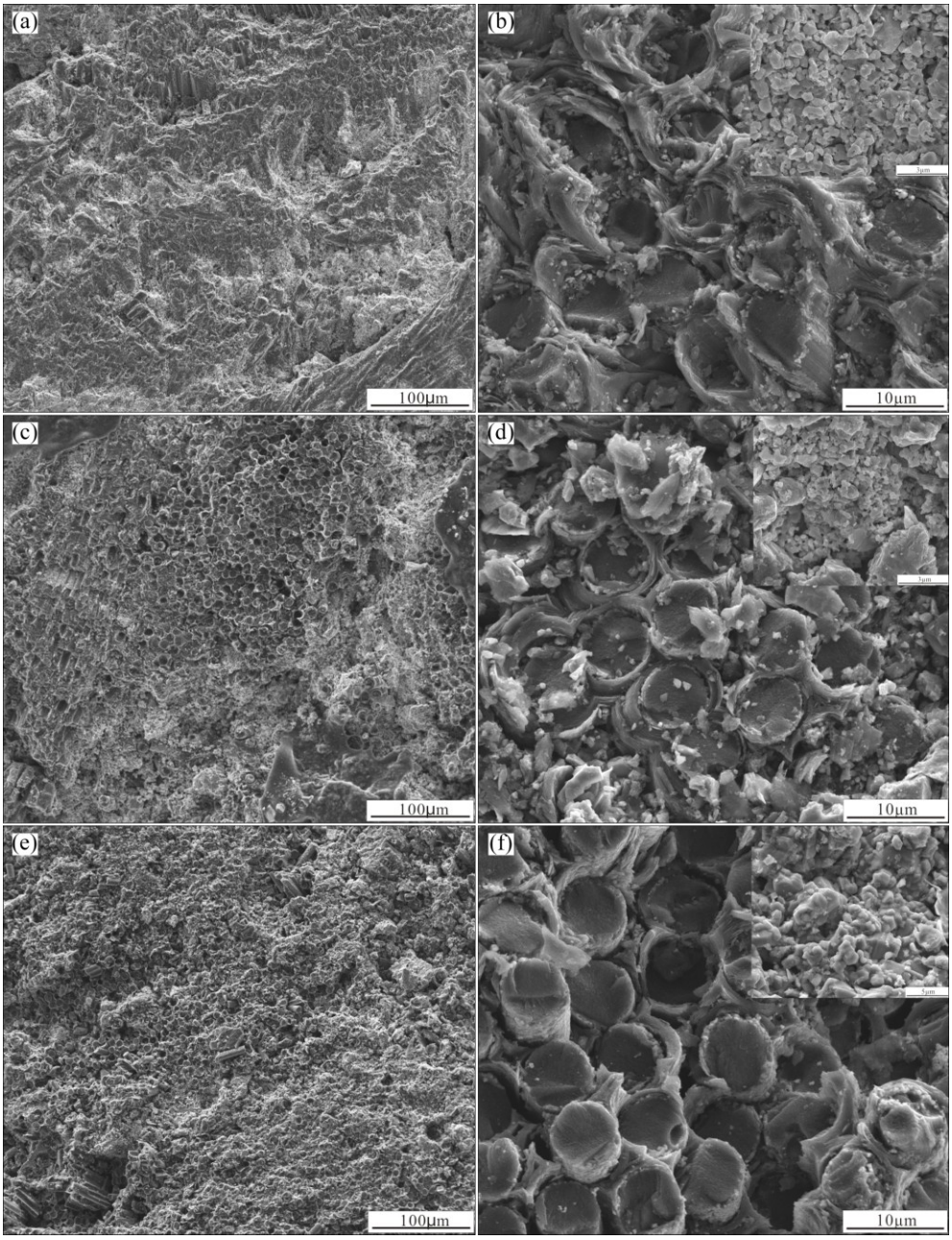

Fig. 2 Microstructures of C/C−SiC and C/C−ZrC−SiC composites: (a, b) CSZ-H; (c, d) CSZ-L; (e, f) C/C−SiC

beneficial for retarding oxygen and thermal diffusion to the underlying material.

3.2 Ablation properties

The ablation properties of the prepared composites were evaluated by a plasma generator, and the ablation results of the composites after 60 s plasma torch tests were summarized in Table 1. It can be concluded that these composites reveal outstanding ablation resistance, and the ablation resistance descends gradually with the increase of SiC content. As shown in Table 1, the CSZ-H shows the lowest mass and linear ablation rates of −3.51 mg/s and −1.88 μm/s, respectively. CSZ-L with a higher content of SiC and a lower content of ZrC has a mass ablation rate of −1.57 mg/s and a linear ablation rate of 0.37 μm/s, which are still better than those of the C/C−SiC composites. The C/C−SiC composite exhibits the weakest ablation property with the mass and linear ablation rates of 0.04 mg/s and 1.35 μm/s among all the prepared composites. It can be seen that the changes of mass and linear ablation rates of the composites are quite different, some are increased and some are decreased after ablation. The reason for the discrepancy of the ablation rates will be discussed later combined with the ablation morphology. Moreover, the good ablation resistance of CSZ-H may be related to the higher ZrC and total ceramic content in the matrix.

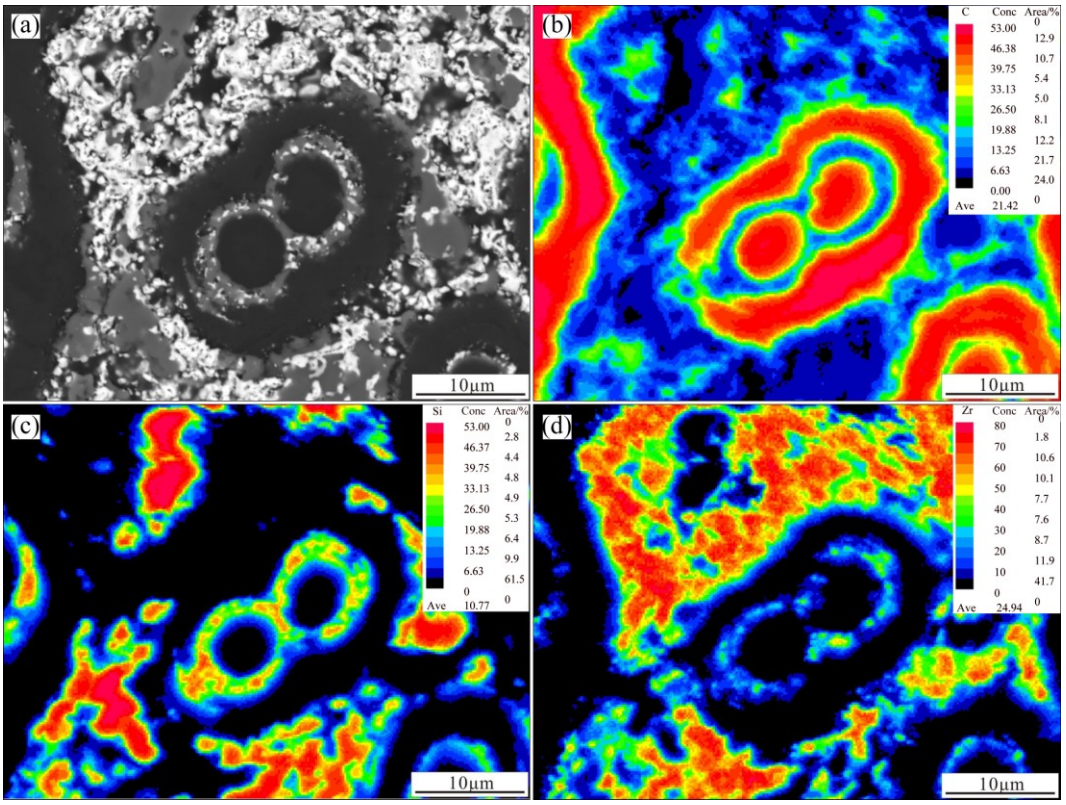

Fig. 3 Cross-section morphology and elemental analysis results of CSZ-H: (a) Morphology; (b) C distribution; (c) Si distribution; (d) Zr distribution

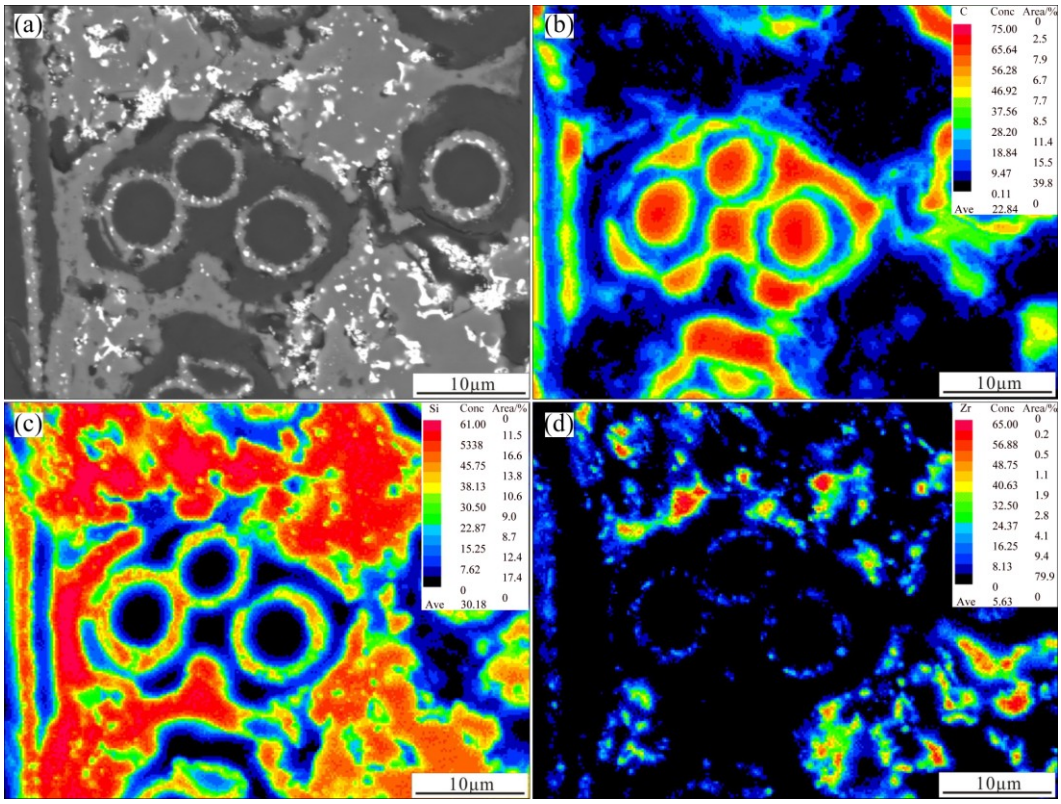

Fig. 4 Cross-section morphology and elemental analysis results of CSZ-L: (a) Morphology; (b) C distribution; (c) Si distribution; (d) Zr distribution

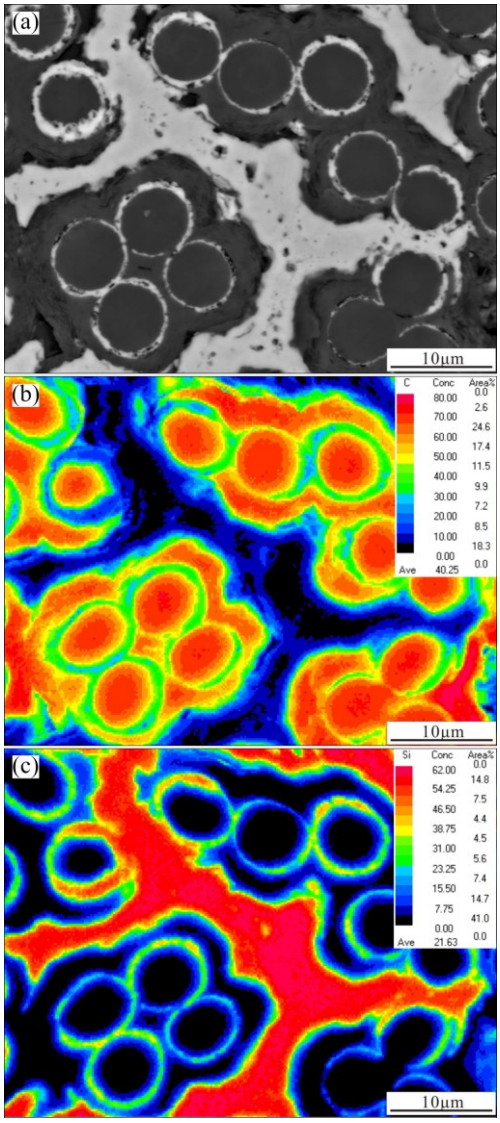

Fig. 5 Cross-section morphology and elemental analysis results of C/C−SiC: (a) Morphology; (b) C distribution; (c) Si distribution

3.3 Ablation morphology

The ablation performance is reflected in the ablated surface morphology besides the ablation rates. Figure 6 shows the photographs of the three prepared composites before and after ablation. It can be seen that the surface remains intact without obvious pores or pits after ablation of C/C−ZrC−SiC composites (Figs. 6(d) and (e)), but a slight ablation crater can be found on the center of C/C−SiC composites (Fig. 6(f)). The surface of the composites is covered with a white dense layer in CSZ-H from Fig. 6(d), while only a small amount of white product covers the central area of CSZ-L from Fig. 6(e).

Figure 7 shows the surface morphologies and EDS of CSZ-H after ablation. As shown in Fig. 7(a), the surface of CSZ-H was covered by a relatively continuous oxide layer with some pores. It is obvious that there are three different morphologies composed of C−O−Si−Zr phase with different mole ratios from Figs. 7(b)−(e). Combined with the results of XRD (Fig. 1) and EDS (Fig. 7(c)−(e)), the grayish-white particulate oxides are mainly composed of ZrO_2 and ZrC with little SiO_2, while the gray glass-like oxides are composed of SiO_2 and ZrO_2 with a ratio about 5:2. It should be noted that the solution of SiO_2 in ZrO_2 would result in a lower melting point of ZrO_2, so the molten ZrO_2 was formed [28]. Although the mole ratio of C−O−Si−Zr in spectrum 1 is close to that in spectrum 2, the appearance of the two regions is different. So it can be supposed that the phase is different between the grayish-white molten oxides and particulate oxides. The Zr−Si−O molten oxides may be a mesophase of SiO_2 and ZrO_2. In addition, the grayish-white oxides scales are mainly distributed outside the glass-like phase due to the viscosity of glass-like SiO_2−ZrO_2 is relatively lower during the ablation, which could seal the surface micro-pores and micro-cracks of the composites. Thereby, the oxides layers can protect the carbon fiber and matrix underearth from further ablation.

Figure 8 shows the surface morphologies and EDS of CSZ-L after ablation. The surface also formed a grayish-white oxide layer (Fig. 8(a)), while the oxide layer is loose in comparison with CSZ-H (Fig. 7(a)). A further observation was conducted on the surface of CSZ-L after ablation. It can be found that a gray glass-like layer with some micro-cracks exists under the loose scale as illustrated in Fig. 8(b). Compared with CSZ-H, the surface of CSZ-L just contains two different phases (white ZrO_2 with a little amount of SiO_2 oxides from Fig. 8(c) and gray glass-like oxides). Furthermore, the gray glass-like phases in CSZ-L are likely composed of SiO_2−SiC with a small amount of ZrO_2 (confirmed by EDS in Fig. 8(d)), which differs from the CSZ-H. These differences between CSZ-H and CSZ-L are attributed to the contents of ZrC and SiC. It has enough ZrC to convert into continuous ZrO_2 scales in CSZ-H, while the content of ZrC is less in CSZ-L. Moreover, The SiC is surplus to convert into molten SiO_2 in CSZ-L. However,

Table 1 Results of ablation test after 60 s

Sample	Density/ ($g \cdot cm^{-3}$)	w(SiC)/%	w(ZrC)/%	Mole ratio of ZrC/(ZrC+SiC)	Mass ablation rate/($mg \cdot s^{-1}$)	Linear ablation rate/($\mu m \cdot s^{-1}$)
C/C−SiC	1.88	21.42±0.01	0	0	0.04±0.01	1.35±0.02
CSZ-L	2.03	18.77±0.02	10.21±0.01	0.19:1	−1.57±0.07	0.37±0.02
CSZ-H	2.14	7.56±0.02	27.20±0.02	0.58:1	−3.51±0.12	−1.88±0.11

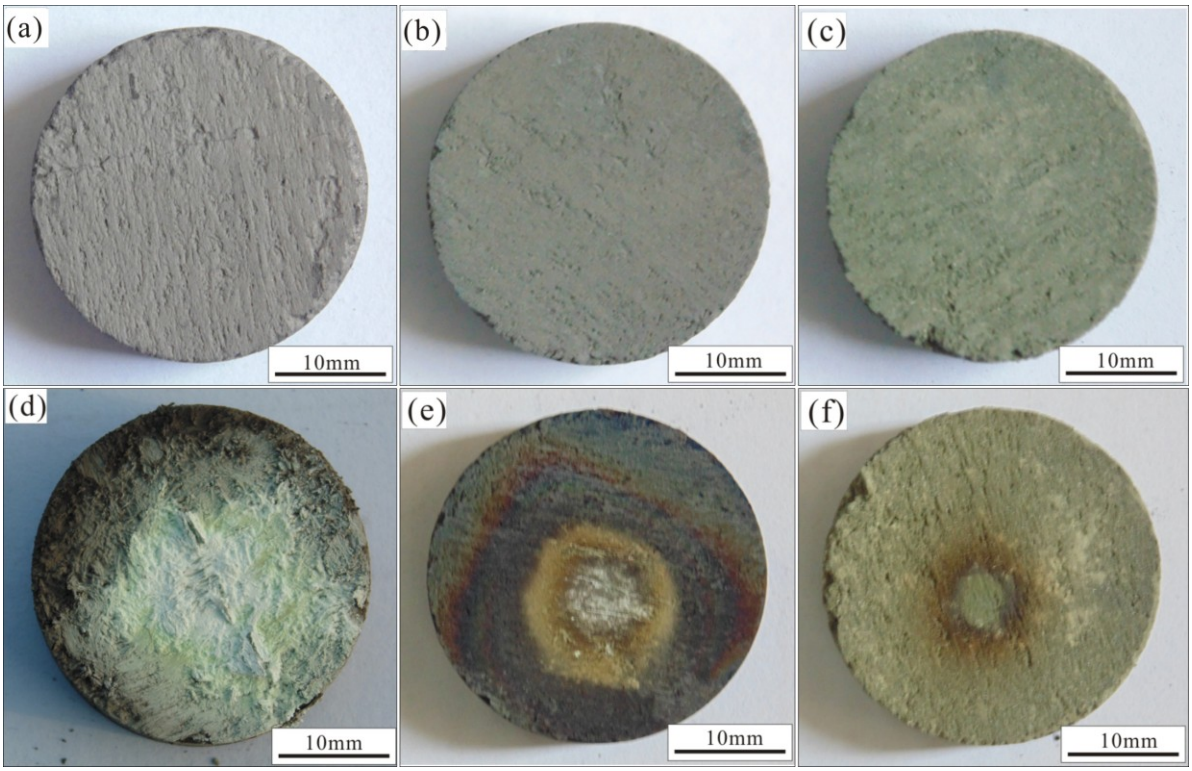

Fig. 6 Photographs of prepared composites before and after ablation: (a, d) CSZ-H; (b, e) CSZ-L; (c, f) C/C−SiC composites

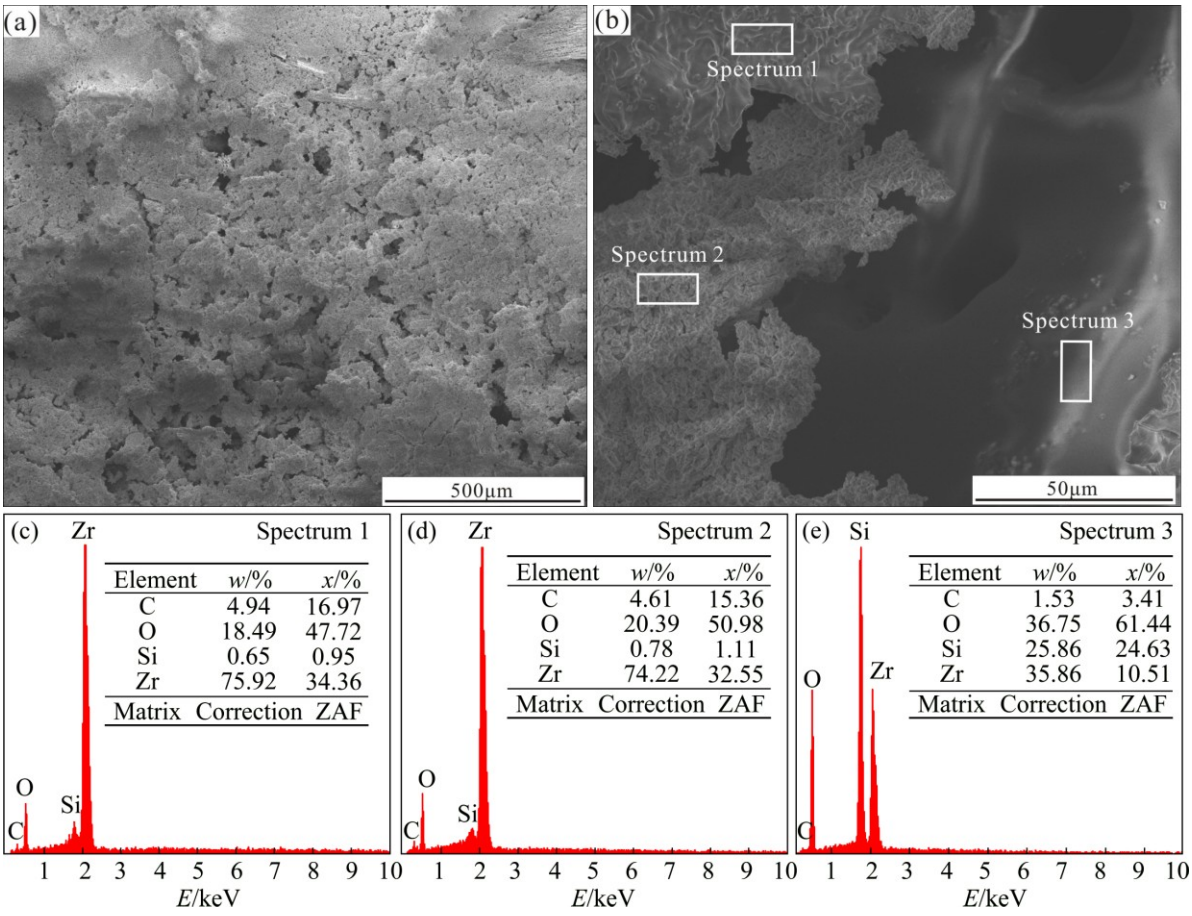

Fig. 7 Surface morphologies and EDS of CSZ-H after ablation: (a) Oxides scale of central region; (b) Solid-liquid coexistence zone; (c) EDS of spectrum 1 in (b); (d) EDS of spectrum 2 in (b); (e) EDS of spectrum 3 in (b)

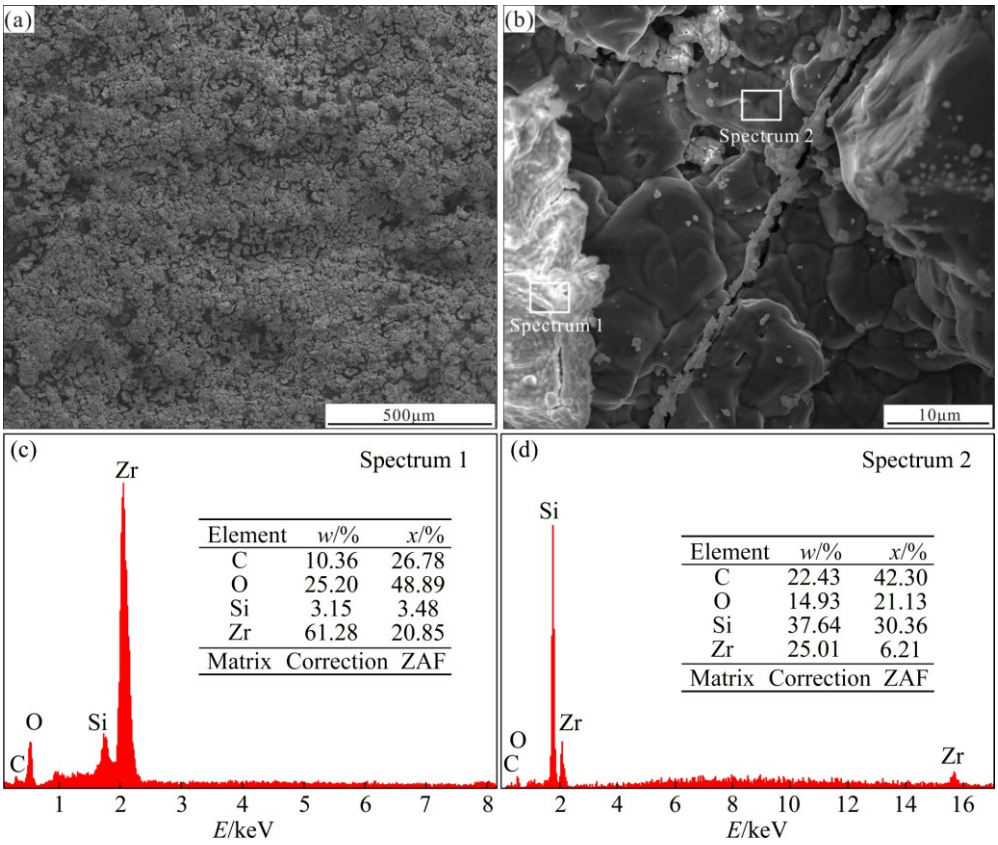

Fig. 8 Surface micro-morphologies and EDS of CSZ-L after ablation: (a) Oxides scale of central region; (b) Central molten region; (c) EDS of spectrum 1 in (b); (d) EDS of spectrum 2 in (b)

the molten glass-like layer connected to the white layer also acted as a barrier of oxidizing species and heat inward diffusion to the composites, which can effectively improve the anti-ablation property of the composites.

The surface morphologies and EDS of C/C−SiC composites are displayed in Fig. 9. It can be seen that a gray scale with some pores was formed on the surface of C/C−SiC composites in Fig. 9(a). Based on the EDS results (Figs. 9(c) and (d)), the gray scale was composed of molten SiO_2 and some SiC solid particles. It is noteworthy that the SiC particles were encapsulated by molten SiO_2 in Fig. 9(a). It is known that the ablation flame temperature exceeds the melting point of SiO_2 and does not reach the sublimation temperature of SiC. And the SiC particle was not oxidized to SiO_2 completely in such a short time. Therefore, some SiC particles are covered by the flowing molten SiO_2. It can be found that the molten SiO_2 layer is rough and there are some pores in the oxide layer from Fig. 9(b), due to the scouring of the combustion gas and the evaporation of SiO and SiO_2. These pores would become the diffusion channel for oxidizing species to erode the composites.

It is known that the oxidation of ZrC−SiC into ZrO_2−SiO_2 will increase the mass/volume of the ceramics, while the oxidation of C will cause the decrease of mass/volume of the composites. So, the formation of continuous ZrO_2−SiO_2 protective layer will increase the mass/thickness of the composites [15]. According to the morphology of these composites after ablation, the oxides layer on CSZ-H is relatively continuous, while the oxides layer of CSZ-L is looser than CSZ-H. Moreover, the oxides layer of C/C−SiC composites shows the worst scouring resistance. All these phenomena resulted in the discrepancy of the mass/linear ablation rates of these composites (Table 1).

It can be concluded from the morphologies of CSZ-H, CSZ-L and C/C−SiC composites that the solid ZrO_2−ZrC ceramics play a role of pinning the molten SiO_2 that can decline the denudation of high-speed flame. Simultaneously, the molten SiO_2 would adhere the dispersed solid ceramics besides sealing the voids and micro-cracks.

3.4 Ablation mechanism

A series of complex thermal-chemical, thermal-physical and mechanical denudation processes occurred during the ablation process of the prepared composites. The thermal-chemical process involves the reactions of oxidizing species with SiC, ZrC, carbon fiber and pyrocarbon, etc. The thermal-physical means the melting of SiO_2, the sublimation of SiO_2, and the volume changes of ceramics and matrix. The mechanical denudation

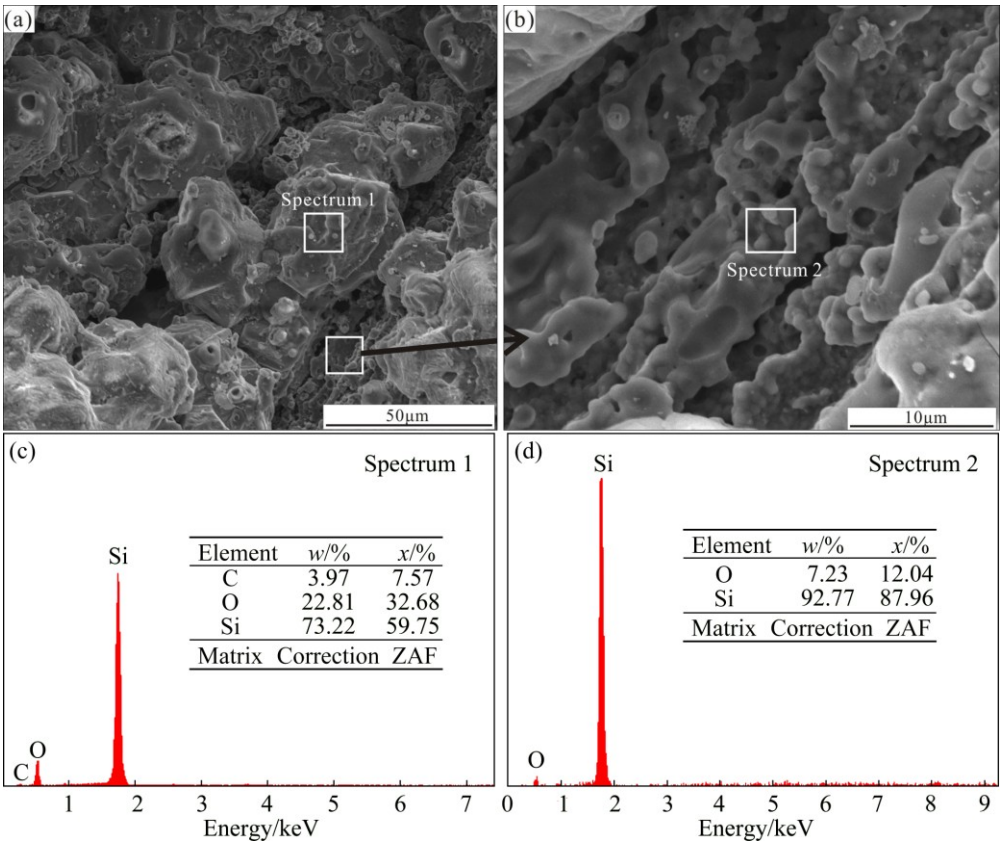

Fig. 9 Surface morphologies and EDS of C/C−SiC composites after ablation: (a) Central region; (b) Formed molten scale; (c, d) EDS of spectra 1 and 2 in (a) and (b), respectively

refers to the peeling of ceramics, carbon matrix and carbon fiber by the shearing forces of the flame with high speed, high pressure and high temperature [29,30].

Based on the different surface morphologies of the prepared composites after ablation, the schematic diagram of ablation model for the composites is shown in Fig. 10. At the beginning of the ablation, carbon fibers, pyrocarbon, SiC and ZrC ceramics were oxidized, then formed a oxide scale rapidly on the surface of the composites. Therefore, the further ablation of the substrate was mainly dominated by the diffusion rate of oxygen through the oxides layer and the intensity of denudation. For the C/C−SiC composites, the oxide scale was mainly composed of SiO_2 with some SiC particles. The molten SiO_2 would cover the surface active sites due to its good self-healing ability, which could promote the ablation resistance of the C/C−SiC composites. However, the formed molten SiO_2 can easily be desquamated by the high speed flame due to the high ablation temperature which exceeds the boiling point of SiO_2 [31,32]. Moreover, the SiO_2 would react with SiC to form gaseous SiO and CO above 1600 °C [33]. These processes would accelerate the ablation of the composites. On the contrary, the ablated ZrO_2 and ZrC ceramics of C/C−ZrC−SiC composites are partially melted during the ablation, which can play a critical role of restricting the mechanical denudation of high velocity combustion gas.

It is well known that the structure and composition of oxide film has a great effect on ablation resistance. While the contents of ZrC and SiC are closely linked with the structure of oxide scales, so the contents of ZrC and SiC have significant impacts on ablation properties. For CSZ-H, the mole ratio of $ZrO_2/(ZrO_2+SiO_2)$ after ablation is about 0.55:1 to 0.61:1 because the mole ratio of ZrC/(ZrC+SiC) is 0.58:1 (Table 1). It would separate out solid phase at 2300 °C according to the binary SiO_2−ZrO_2 phase diagrams from Ref. [34], which is in agreement with Fig. 7(b). The newly precipitated Zr−Si−O phase and the solid ZrC−ZrO_2 could increase the viscosity of SiO_2 moderately, thus improving the ability of resisting mechanical denudation. Moreover, the molten binary ZrO_2−SiO_2 could seal the weak sites on the surface of the composites, so it could significantly improve the anti-ablation property. However, for CSZ-L, the mole ratio of $ZrO_2/(ZrO_2+SiO_2)$ is located in liquid region of the SiO_2−ZrO_2 phase diagrams at 2300 °C [34], so it would form large amount of liquid products during the ablation. Otherwise, the amount of unmelted ZrO_2 in CSZ-L is lower compared with CSZ-H. In this case, the

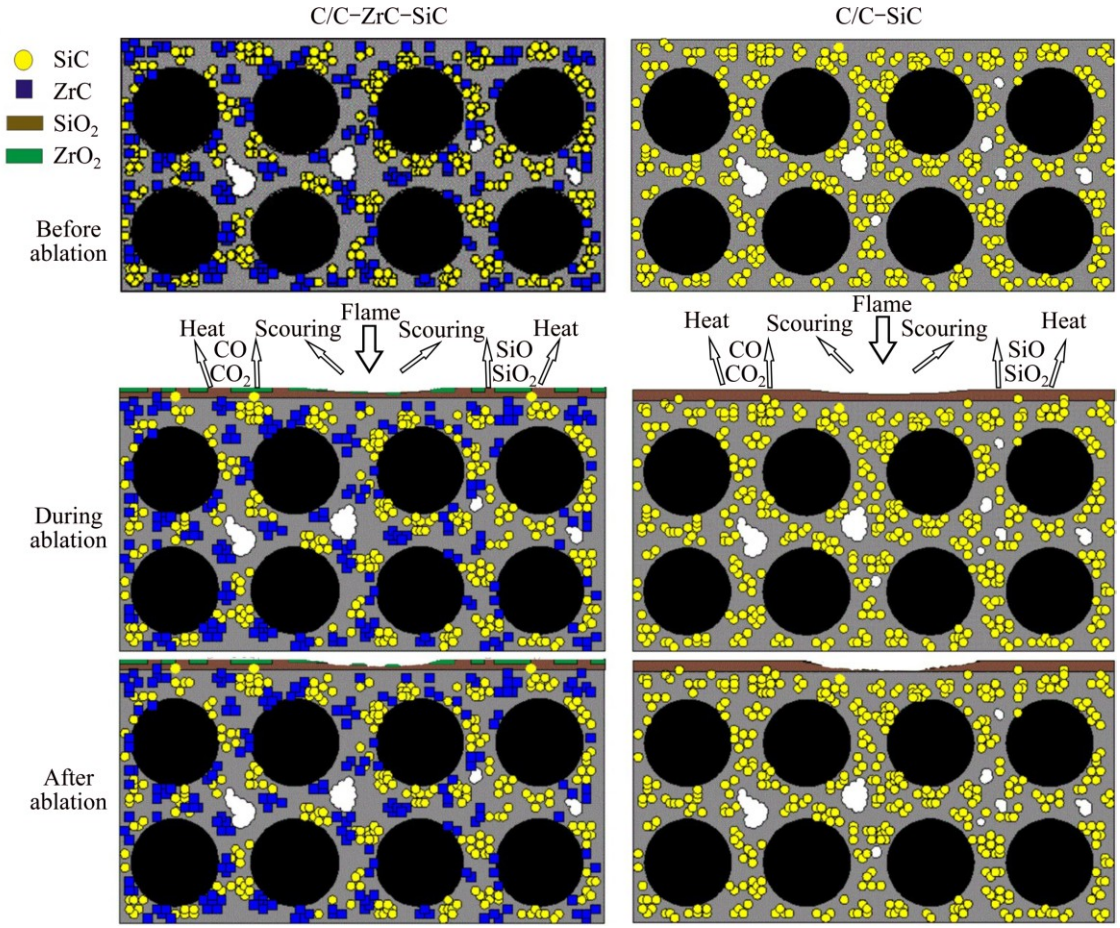

Fig. 10 Schematic diagram of ablation model for composites

evaporation and peeling of molten products become serious, which have a bad effect on the ablation resistance. As a result, the ablation is more severe when the content of ZrC is lower.

According to above discussion, on one hand, the partially melted ZrO_2−ZrC and molten SiO_2 can improve the strength of oxide film, which could enhance the anti-scouring ability of the composites. On the other hand, the continuous scale with molten ZrO_2−SiO_2 sealing the weak sites can restrain the diffusion rate of oxygen and heat infiltrated into the substrate.

4 Conclusions

1) The C/C−SiC and C/C−ZrC−SiC composites with different SiC−ZrC contents were fabricated by PIP via using SiC and ZrC precursors separately.

2) The content of ZrC−SiC has significant effects on microstructure and ablation resistance. With increasing of ZrC, the composites show a higher density and fewer closed pores in the intra-bundle areas, and some SiC and ZrC ceramics were embedded circle-around carbon fiber.

3) The ablation resistance descends gradually with the decrease of ZrC content. The C/C−SiC composit shows the weakest ablation property, while the CSZ-H exhibits the lowest ablation rates.

4) In the ablation process, the high ZrC content is beneficial for separating out a solid Zr−Si−O phase and forms a more continuous and denser ceramic oxide scale. The solid Zr−Si−O phase could increase the viscosity of SiO_2 moderately, thus improving the ability of resisting mechanical denudation. Moreover, the continuous integrate SiO_2−ZrO_2−ZrC−SiC layer would serve as the barrier of thermal and oxygen diffusion, which can prevent the substrate from further ablation.

References

[1] DIETRICH S, GEBERT J M, STASIUK G, WANNER A, WEIDENMANN K A, DEUTSCHMANN O, TSUKROV I, PIAT R. Microstructure characterization of CVI-densified carbon/carbon composites with various fiber distributions [J]. Composites Science and Technology, 2012, 72(15): 1892−1900.

[2] FANG Hua-chan, XIAO Peng, XIONG Xiang, YU Guang-jun. Microstructures, mechanical and oxidation behaviors of C/C composites modified by NiAl alloy [J]. Transactions of Nonferrous Metals Society of China, 2016, 26(1): 196−202.

[3] ZAMAN W, LI K Z, IKRAM S, LI W. Residual compressive and thermophysical properties of 4D carbon/carbon composites after repeated ablation under oxyacetylene flame of 3000 °C [J]. Transactions of Nonferrous Metals Society of China, 2013, 23(6): 1661−1667.

[4] ZENG Yi, XIONG Xiang, LI Guo-dong, CHEN Zhao-ke, SUN Wei, WANG Di-ni. Microstructure and ablation behavior of carbon/carbon composites infiltrated with Zr−Ti [J]. Carbon, 2013, 54: 300−309.

[5] SUN Can, LI He-jun, FU Qian-gang, ZHANG Jia-ping, PENG Han. Double SiC coating on carbon/carbon composites against oxidation by a two-step method [J]. Transactions of Nonferrous Metals Society of China, 2013, 23(7): 2107−2112.

[6] ZAPATA S E, JAYASEELAN D D, BROWN P M, LEE W E. Effect of La_2O_3 addition on long-term oxidation kinetics of ZrB_2−SiC and HfB_2-SiC ultra-high temperature ceramics [J]. Journal of the European Ceramic Society, 2014, 34(15): 3535−3548.

[7] JAMES E S. Oxidation protection for carbon fiber composites [J]. Carbon, 1989, 27(5): 709−715.

[8] YANG Xin, SU Zhe-an, HUANG Qi-zhong. CHAI Li-yuan. Preparation and oxidation resistance of mullite/SiC coating for carbon materials at 1150 °C [J]. Transactions of Nonferrous Metals Society of China, 2012, 22(12): 2997−3002.

[9] PAUL A, VENUGOPAL S, BINNER J G P, VAIDHYANATHAN B, HEATON A C J, BROWN P M. UHTC-carbon fibre composites: Preparation, oxyacetylene torch testing and characterisation [J]. Journal of the European Ceramic Society, 2013, 33(2): 423−432.

[10] GE Yi-cheng, YANG Ling-yun, WU Shuai, LI Chan, LUO Jian, YI Mao-zhong. Influence of heat-treatment on oxidation-resistance of phosphate-coating for C/C composite [J]. Transactions of Nonferrous Metals Society of China, 2014, 24(2): 455−461.

[11] ELSHEIKH S M, ZAKI Z I, AHMED Y M Z. In situ synthesis of ZrC/SiC nanocomposite via carbothermic reduction of binary xerogel [J]. Journal of Alloys and Compounds, 2014, 613: 379−386.

[12] LIU Chun-xuan, CHEN Jian-xun, SU Zhe-an, YANG Xin, CAO Liu-xu, HUANG Qing-zhong. Pyrolysis mechanism of ZrC precursor and fabrication of C/C−ZrC composites by precursor infiltration and pyrolysis [J]. Transactions of Nonferrous Metals Society of China, 2014, 24(6): 1779−1784.

[13] LIU Chun-xuan, CAO Liu-xu, CHEN Jian-xun, XUE Liang, TANG Xian, HUANG Qi-zhong. Microstructure and ablation behavior of SiC coated C/C−SiC−ZrC composites prepared by a hybrid infiltration process [J]. Carbon, 2013, 65: 196−205.

[14] XIE Jing, LI Ke-zhi, LI He-jun, FU Qian-gang, GUO Ling-jun. Ablation behavior and mechanism of C/C−ZrC−SiC composites under an oxyacetylene torch at 3000 °C [J]. Ceramics International, 2013, 39(4): 4171−4178.

[15] XIE Jing, LI Ke-zhi, LI He-jun, FU Qian-gang, LIU Lei. Cyclic ablation behavior of C/C−ZrC−SiC composites under oxyacetylene torch [J]. Ceramics International, 2014, 40(4): 5165−5171.

[16] LI Qing-gang, DONG Shao-ming, WANG Zhi, SHI Guo-pu. Fabrication and properties of 3D C_f/ZrC-SiC composites by the vapor silicon infiltration process [J]. Ceramics International, 2013, 39(4): 4723−4727.

[17] YANG Xin, SU Zhe-an, HUANG Qi-zhong, FANG Xiao, CHAI Li-yuan. Microstructure and mechanical properties of C/C−ZrC−SiC composites fabricated by reactive melt infiltration with Zr, Si mixed powders [J]. Journal of Materials Science & Technology, 2013, 29(8): 702−710.

[18] ZHANG Liang-run, DONG Shao-ming, ZHOU Hai-jun, KAN Yan-mei, ZHOU Fan, WANG Zhen. 3D C_f/ZrC−SiC composites fabricated with ZrC nanoparticles and $ZrSi_2$ alloy [J]. Ceramics International, 2014, 40(8): 11795−11801.

[19] LIU Chun-xuan, SU Zhe-an, HUANG Qi-zhong, CHEN Jian-xun, YANG Xin, CAO Liu-xu, YIN Teng, ZHONG Ping. Ablation behavior of ZrC−SiC coated C/C−ZrC−SiC composites prepared by precursor infiltration pyrolysis combined with reactive melt infiltration [J]. Journal of Alloys and Compounds, 2014, 597: 236−242.

[20] FENG Bo, LI He-jun, ZHANG Yu-lei, LIU Lei, YAN Min. Effect of SiC/ZrC ratio on the mechanical and ablation properties of C/C−SiC−ZrC composites [J]. Corrosion Science, 2014, 82: 27−35.

[21] YAN Chun-lei, LIU Rong-jun, CAO Ying-bin, ZHANG Chang-rui, ZHANG De-ke. Ablation behavior and mechanism of C/ZrC, C/ZrC−SiC and C/SiC composites fabricated by polymer infiltration and pyrolysis process [J]. Corrosion Science, 2014, 86: 131−141.

[22] CHEN Si-an, HU Hai-feng, ZHANG Yu-di, ZHANG Chang-rui, WANG Qi-kun. Effects of TaC amount on the properties of 2D C/SiC−TaC composites prepared via precursor infiltration and pyrolysis [J]. Materials & Design, 2013, 51: 19−24.

[23] CHEN Zhao-feng, FANG Dan, MIAO Yun-liang, YAN Bo. Comparison of morphology and microstructure of ablation centre of C/SiC composites by oxy-acetylene torch at 2900 and 3550 °C [J]. Corrosion Science, 2008, 50(12): 3378−3381.

[24] XUE Liang, SU Zhe-an, YANG Xin, HUANG Dong, YIN Teng, LIU Chun-xuan. HUANG Qi-zhong. Microstructure and ablation behavior of C/C−HfC composites prepared by precursor infiltration and pyrolysis [J]. Corrosion Science, 2015, 94: 165−170.

[25] LI He-jun, LIU Lei, ZHANG Yu-dan, LI Ke-zhi, SHI Xiao-hong, ZHANG Yu-lei, FENG Wei. Effect of high temperature heat treatment on the ablation of SiC−ZrB_2−ZrC particles modified C/C composites in two heat fluxes [J]. Journal of Alloys and Compounds, 2015, 621: 18−25.

[26] YAN Chun-lei, LIU Rong-jun, CAO Ying-bin. ZHANG Chang-rui. Fabrication and properties of PIP 3D C_f/ZrC−SiC composites [J]. Materials Science and Engineering A, 2014, 591: 105−110.

[27] WANG Pei, ZHANG Shou-yang, LI He-jun, KONG Jie, LI Wei, ZAMAN W. Variation of thermal expansion of carbon/carbon composites from 850 to 2500 °C [J]. Ceramics International, 2014, 40(1): 1273−1276.

[28] HAN Jie-cai, HU Ping, ZHANG Xing-hong, MENG Song-he, HAN Wen-bo. Oxidation-resistant ZrB_2−SiC composites at 2200 °C [J]. Composites Science and Technology, 2008, 68: 799−806.

[29] LI Cui-yan, LI Ke-zhi, LI He-jun, ZHANG Yu-lei, OUYANG Hai-bo, YAO Dong-jia, LIU Lei. Microstructure and ablation resistance of carbon/carbon composites with a zirconium carbide rich surface layer [J]. Corrosion Science, 2014, 85: 160−166.

[30] SHEN Xue-tao, LI Ke-zhi, LI He-jun, DU Hong-ying, CAO Wei-feng, LAN Feng-tao. Microstructure and ablation properties of zirconium carbide doped carbon/carbon composites [J]. Carbon, 2010, 48(2): 344−351.

[31] YANG Xin, HUANG Qi-zhong, SU Zhe-an, CHANG Xin, CHAI Li-yuan, LIU Chun-xuan, XUE Liang, HUANG Dong. Resistance to oxidation and ablation of SiC coating on graphite prepared by chemical vapor reaction [J]. Corrosion Science, 2013, 75: 16−27.

[32] HUANG Dong, ZHANG Ming-yu, HUANG Qi-zhong, WANG Li-ping, TANG Xian, YANG Xin, TONG Kai. Fabrication and ablation property of carbon/carbon composites with novel SiC−ZrB_2 coating [J]. Transactions of Nonferrous Metals Society of China, 2015, 25(11): 3708−3715.

[33] FAHRENHOLTZ W G. Thermodynamic analysis of ZrB_2−SiC oxidation: Formation of a SiC-depleted region [J]. Journal of the American Ceramic Society, 2007, 90(1): 143−148.

[34] BALL R G J, MIGNANELLI M A, BARRY T I, GISBY J A. The calculation of phase equilibria of oxide core-concrete systems [J]. Journal of Nuclear Materials, 1993, 201: 238−249.

ZrC−SiC 含量对 C/C 复合材料显微结构和烧蚀性能的影响

李 军，杨 鑫，苏哲安，薛 亮，钟 平，李帅鹏，黄启忠，刘红卫

中南大学 粉末冶金国家重点实验室，长沙 410083

摘 要：通过先驱体浸渍裂解法制备了不同 ZrC−SiC 含量的 C/C−ZrC−SiC 复合材料，并研究了不同陶瓷含量对材料显微结构和烧蚀性能的影响。C/C−SiC 和 C/C−ZrC−SiC 复合材料在 2300 ℃ 的烧蚀火焰下均呈现出优异的抗烧蚀性能。随着 ZrC 陶瓷含量的增加，在烧蚀过程中形成了连续的氧化膜涂层及固态的 Zr−Si−O 中间相，并且氧化物薄膜的结构与 ZrC−SiC 陶瓷的含量密切相关。固态的 ZrO_2−ZrC 和 Zr−Si−O 中间相可以适当提高 SiO_2 的黏度，从而提升氧化膜的抗剥蚀能力。连续的 SiO_2−ZrO_2−ZrC−SiC 层将作为热量和氧气的扩散障碍层，阻止其向材料内部扩散而引起材料的进一步烧蚀。ZrC 和 SiC 含量分别为 27.2%和 7.56%时，C/C−ZrC−SiC 复合材料表现出更好的抗烧蚀性能，其质量烧蚀率和线烧蚀率分别为−3.51 mg/s 和−1.88 μm/s。

关键词：C/C 复合材料；ZrC；SiC；烧蚀；先驱体浸渍裂解法

(Edited by Yun-bin HE)